JOURNAL OF PROPULSION AND POWER
Vol. 26, No. 1, January–February 2010

Resonant Response of Mistuned Bladed Disks Including Aerodynamic Damping Effects

Yoon S. Choi,* Dana A. Gottfried,† and Sanford Fleeter‡
Purdue University, West Lafayette, Indiana 47907

DOI: 10.2514/1.36537

A mathematical model is developed to investigate the effects of aerodynamic damping on the maximum amplification factor of mistuned bladed disks. LINSUB, an inviscid linearized unsteady aerodynamic damping code, provides aerodynamic damping influence coefficients that are incorporated into a partial-mistuning model that takes advantage of mode localization. This mistuning analysis is then used to demonstrate the effects of aerodynamic damping on the maximum amplification factor of mistuned bladed disks. The relative importance of aerodynamic effects is determined by a comparison of aerodynamic damping and structural damping factors. It is shown that neglecting unsteady aerodynamics may result in the predicted optimal mistuning pattern not being optimum in the actual operating environment wherein unsteady aerodynamic effects are present.

Nomenclature

$\hat{C}_j^k$	=	aerodynamic influence of the motion of airfoil k on airfoil j
$C(\beta_r)$	=	unsteady aerodynamic coefficient
c	=	airfoil chord length
$\underline{h}^k$	=	tuned response to single airfoil forcing on airfoil k
k	=	reduced frequency, $\omega c/U$
k_c	=	structural coupling stiffness
k_j	=	structural stiffness of airfoil j
k_t	=	mean or tuned structural stiffness
L_j	=	generalized aerodynamic force of airfoil j
m	=	generalized inertia per unit span
N	=	number of airfoils in row
ND	=	nodal diameter
r	=	engine order of excitation
s	=	number of airfoils affected by mistuning
u	=	fluid velocity
X	=	generalized displacement
β_r	=	interblade phase angle, $2\pi r/N$
Γ_j^k	=	dimensional aerodynamic influence coefficient
δk_j	=	mistuned stiffness of airfoil j
ρ	=	fluid density
ζ^{mech}	=	dimensionless mechanical damping factor
ζ^{aero}	=	dimensionless aerodynamic damping factor
ω_r	=	resonant frequency of airfoil row

Superscripts

d	=	directly affected by mistuning
i	=	indirectly affected by mistuning
t	=	tuned

Presented as Paper 4977 at the 39th AIAA/ASME/SAE/ASEE Joint Propulsion Conference and Exhibit, Huntsville, AL, 20–23 July 2003; received 8 January 2008; revision received 20 July 2009; accepted for publication 20 July 2009.

*Graduate Research Assistant, Mechanical Engineering, 500 Allison Road. Student Member AIAA.

†Postdoctoral Researcher, Mechanical Engineering, 500 Allison Road. Member AIAA.

‡McAllister Distinguished Professor, Mechanical Engineering, 500 Allison Road. Fellow AIAA.

I. Introduction

HIGH cycle fatigue (HCF) of turbomachine blading resulting from flow-induced vibration is a significant problem throughout the gas turbine industry. To address this problem, various approaches have been developed to predict airfoil resonant response. In these, the response of a tuned airfoil row, that is, a rotor with all airfoils having the same structural properties and thus identical natural frequencies, is analyzed.

In fact, there are small airfoil-to-airfoil structural property variations that result, for example, from the manufacturing process or as a consequence of in-service wear. These are collectively referred to as mistuning and are known to lead to significant increases in airfoil resonant response amplitude as compared to that of the tuned airfoil row, with mistuning thus often cited as an HCF source. Hence, the key metric that characterizes the resonant response of mistuned bladed disks is the amplification factor, the ratio of the largest response amplitude of a mistuned bladed disk to that of a tuned bladed disk.

The earliest mistuning analyses were deterministic and used simplified models to produce closed-form expressions to bound the mistuned rotor maximum response [1,2]. More recently, Kenyon and Griffin developed a more general analysis that recovers earlier closed-form expressions as special cases [3]. Direct numerical optimization to estimate the maximal response over a set of mistuning variations is an alternative deterministic approach [4,5]. Of particular interest herein is the mistuning model developed by Rivas-Guerra and Mignolet that takes advantage of mode localization by only considering a few airfoils on the rotor, that is, airfoils far from the maximum amplitude airfoil can be considered as tuned airfoils [6]. This partial-mistuning model results in a reduction in the number of variables in the optimization procedure to determine the mistuning pattern that results in the largest amplification factor.

One significant phenomenon not addressed in these mistuning models is the airfoil row unsteady aerodynamics. Because damping is known to be the important parameter controlling maximum resonant response amplitude, it might be expected that the unsteady aerodynamics resulting from the vibration of the blading itself, specifically the aerodynamic damping, will have a significant effect on the resonant response amplitude of tuned and mistuned bladed disks. Note that the mechanical damping is considerably reduced in newer rotor designs, particularly those with integral bladed rotors (IBRs) and those without shrouds. As a result, it is anticipated that aerodynamic damping will be particularly important in the vibratory stress analysis of IBRs. Specifically, IBRs inherently have very low mechanical damping as compared to a traditional bladed rotor. This very low mechanical damping of IBRs implies that they are highly susceptible to HCF and also that aerodynamic damping is a

significant component of the IBR damping and, thus, an important consideration.

Two families of techniques are used to predict aerodynamic damping of blade rows: time marching and time linearized. Time-marching techniques applied to the fluid equations are the most widely used. In time-linearized analyses, the fluid equations are linearized by considering the flow unsteadiness to be small compared to the mean flow. The resulting small disturbance equations are then solved assuming that the disturbance flow is harmonic with a constant interblade phase angle between adjacent blades. Time-linearized models are computationally very efficient as compared to time-marching ones. Thus, they are well suited for use in a mistuning simulation, which is directed at determining the maximum amplification factor of a mistuned rotor.

Unfortunately, the basic assumptions inherent in both time-marching and linearized unsteady aerodynamic damping analyses are too restrictive for mistuning simulations. Specifically, the airfoils are required to oscillate harmonically with uniform amplitude and a constant phase relationship or interblade phase angle between airfoils. However, if there are airfoil-to-airfoil material differences, that is, mistuning, the mistuned airfoils respond in modal patterns that violate the assumptions of uniform vibration amplitude and interblade phase angle.

The vibration of mistuned bladed disks with both structural and aerodynamic coupling has been examined [7–13]. However, recently developed reduced-order modeling methods provide a new opportunity to investigate this issue more thoroughly. The component mode mistuning [14] (CMM) and subset of nominal system modes [15] formulations were presented with unsteady aerodynamic terms included in the system equations of motion. Research has been recently initiated by Kielb et al. [16] using the FMM method and He et al. [17] using the CMM method.

This paper is directed at investigating the effects of aerodynamic damping on the amplification factor of mistuned rotors. First, the restrictions of uniform blade vibration amplitude and constant interblade phase angle are removed, accomplished by determining the influence coefficients that characterize the aerodynamic damping of each airfoil oscillating with its own unique amplitude. This aerodynamic damping influence coefficient analysis is then incorporated into a lumped parameter mistuning model that takes advantage of mode localization by considering any specified number of airfoils on the row. This mistuning analysis including unsteady aerodynamic damping is then used to demonstrate the effects of aerodynamic damping on the maximum amplification factor of mistuned rotors.

II. Unsteady Aerodynamic Model

LINSUB [18] is a semi-analytic unsteady aerodynamic model for turbomachinery geometries. The model simplifies the turbomachinery blade row to a two-dimensional cascade of flat plate airfoils, with the flow unsteadiness a small perturbation from the uniform steady flow. Under these assumptions, LINSUB can model a wide range of unsteady flow phenomena, including self-induced cascade vibrations, cascade response to gusts, and cascade response to upstream-going and downstream-going acoustic waves. In each, the LINSUB model predicts the unsteady pressure on the cascade airfoils as well as the upstream-going and downstream-going acoustic signals created by the cascade.

LINSUB requires six inputs: 1) number of control points on the airfoil np, 2) spacing-to-chord ratio s/c, 3) stagger angle γ, 4) Mach number M, 5) reduced frequency k_c, and 6) interblade phase angle σ. The elastic axis position must also be input, but its value has no effect in this study. The number of control points for all the cases is set to 30, determined by means of a study that demonstrated that round-off error for single-precision LINSUB becomes significant for np much greater than 30.

LINSUB requires the interblade phase angle to be specified as a consequence of the assumption that the airfoils oscillate with uniform amplitude and a known constant phase shift from airfoil to airfoil. In a mistuned bladed disk, the airfoils respond in modal patterns that violate the assumption of uniform amplitude and phase shift. Thus, to predict the unsteady aerodynamics of a mistuned airfoil row, the interblade phase angle restriction must be removed. This is accomplished by means of an unsteady aerodynamic influence coefficient technique [19,20]. Namely, for a given mean flowfield and reduced frequency of oscillation, the cascade unsteady aerodynamics are expressed in terms of linearly combined influence coefficients. These influence coefficients can then be used to predict the unsteady aerodynamics of a mistuned airfoil row.

For a finite cascade with N airfoils executing constant amplitude harmonic oscillations with a constant interblade phase angle β_r, the unsteady aerodynamic lift or moment coefficient $C(\beta_r)$ for the cascade can be expressed as the sum

$$C(\beta_r) = \sum_{k=0}^{N-1} \hat{C}_j^k e^{-i(k-j)\beta_r} \tag{1}$$

where $\hat{C}_j^k$ are the complex unsteady aerodynamic influence coefficients that define the unsteady lift or moment developed on airfoil j due to the motion of airfoil k with all other airfoils stationary.

The term $e^{-i(k-j)\beta_r}$ satisfies the requirement that $C(\beta_r)$ is the lift or moment when all airfoils are oscillating with a constant interblade phase angle $\beta_r = \frac{2\pi r}{N}$, where r is an integer engine order ranging from 0 to $N-1$. Thus, $C(\beta_r)$ has a fundamental period of 2π.

The unsteady aerodynamic influence coefficients $\hat{C}_j^k$ are not known directly, but $C(\beta_r)$ is determined directly from LINSUB. Thus, the $\hat{C}_j^k$ are determined by inverting Eq. (1), that is, multiplying both sides of the equation by $e^{i(k-j)\beta_r}$ and integrating over β_r from 0 to 2π [9]:

$$\hat{C}_j^k = \frac{1}{2\pi} \int_0^{2\pi} C(\beta_r) e^{i(k-j)\beta_r} \, \mathrm{d}\beta_r \tag{2}$$

Integrating with the rectangle rule gives

$$\hat{C}_j^k = \frac{1}{N} \sum_{r=0}^{N-1} C(\beta_r) e^{i(k-j)\beta_r} \tag{3}$$

An example of the moment-due-to-torsion coefficient variation with β_r predicted by LINSUB is shown in Fig. 1. Integrating according to Eq. (3) yields the influence coefficients for airfoil j shown in Fig. 2. As expected, the largest influence comes from airfoil j itself, with the influence of neighboring airfoils quickly decreasing away from airfoil j.

For a tuned airfoil row, $C(\beta_r)$ determined from LINSUB would be sufficient to model aerodynamic effects because the row oscillates with constant interblade phase and amplitude. However, for a mistuned airfoil row, the $\hat{C}_j^k$ are key in providing the unsteady aerodynamic effects when there is no constant phase relation between airfoils and vibration amplitudes differ from airfoil to airfoil.

III. Mathematical Model

The mistuned rotor forced response model including aerodynamic damping and coupling effects is depicted in Fig. 3. Note that k_c is the

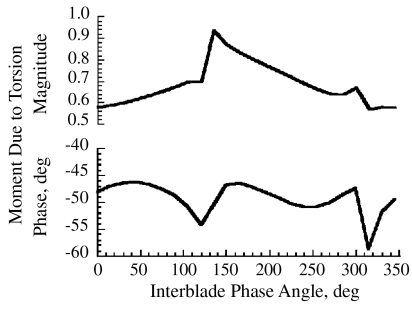

Fig. 1 Moment-due-to-torsion coefficient: LINSUB.

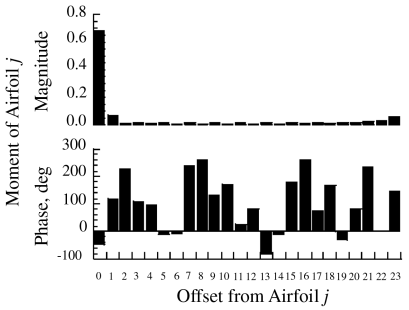

Fig. 2 Influence coefficient.

structural airfoil-to-airfoil coupling stiffness; k_c^{aero} is the unsteady aerodynamic airfoil-to-airfoil coupling stiffness, that is, the real part of the unsteady aerodynamic loading; and ζ^{aero} is the unsteady aerodynamic damping, that is, the imaginary part of the unsteady aerodynamic loading.

The dimensional equation of motion for airfoil j is

$$m\ddot{X}_j + \bar{c}\dot{X}_j + (k_j + 2k_c)X_j - k_c X_{j-1} - k_c X_{j+1} - L_j = F_j(t) \quad (4)$$

where $F_j(t)$ is the forcing function; X_j is the generalized displacement of airfoil j; $\bar{c}$ is the structural damping of airfoil j; k_c is the airfoil-to-airfoil structural coupling stiffness, that is, the effect of the airfoils being coupled to one another through the disk; k_j is the structural stiffness of airfoil j; and L_j is the sum total of aerodynamic forces on airfoil j due to the vibration of each airfoil in the row, with this term including the effects of aerodynamic damping ζ_j^{aero} and aerodynamic coupling stiffness $k_{c_j}^{\text{aero}}$.

Equation (4) applies to a two-dimensional slice through the airfoil row and models any single-degree-of-freedom (SDOF) mode such as bending, torsion, or chordwise bending. For example, if torsion is modeled, m is the moment of inertia, L_j is the aerodynamic moment, $F_j(t)$ is the forcing function specified in terms of time varying moment, and X_j is the angular displacement of airfoil j.

The generalized aerodynamic force depends on the SDOF mode being considered:

$$\begin{aligned} L_j &= \sum_{k=0}^{N-1} [\widehat{C}_j^k]^L \rho u^2 c^2 X_k \qquad \text{Bending} \\ L_j &= \sum_{k=0}^{N-1} [\widehat{C}_j^k]^M \rho u^2 c^2 X_k \qquad \text{Torsion} \\ L_j &= \sum_{k=1}^{N} [\widehat{C}_j^k]^{CW} \rho u^2 c^2 X_k \qquad \text{Chordwise Bending} \end{aligned} \quad (5)$$

where ρ denotes the fluid density, c denotes the airfoil chord, and the superscripts L, M, and CW on the influence coefficients denote lift due to bending, moment due to torsion, and chordwise bending.

An engine order excitation r is considered, with the forcing function expressed as

$$F_j(t) = F_0 e^{i[\omega_r t + (j-1)\beta_r]} \quad (6)$$

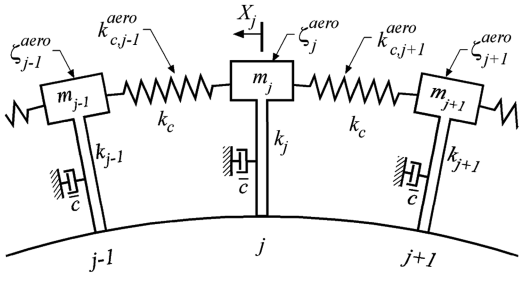

Fig. 3 Airfoil row SDOF model.

where the frequency of excitation equals the natural frequency of the mode.

Neglecting unsteady aerodynamic effects and structural damping yields the natural frequencies of the system in the closed form. Equation (4) can be rewritten as a first-order differential equation:

$$\dot{q} = [D]\underline{q} \quad (7)$$

where $\underline{q} = \{x_1, \dot{x}_1, x_2, \dot{x}_2, \ldots, x_N, \dot{x}_N\}^T$.

The system matrix $[D]$ can be expressed as

$$[D] = \begin{bmatrix} D_1 & D_2 & D_3 & \cdots & D_N \\ D_N & D_1 & D_2 & \cdots & D_{N-1} \\ D_{N-1} & D_N & D_1 & \cdots & D_{N-2} \\ \vdots & \vdots & \vdots & \ddots & \vdots \\ D_2 & D_3 & D_4 & \cdots & D_1 \end{bmatrix} = \begin{bmatrix} A & B & 0 & \cdots & B \\ B & A & B & \cdots & 0 \\ 0 & B & A & \cdots & 0 \\ \vdots & \vdots & \vdots & \ddots & \vdots \\ B & 0 & 0 & \cdots & A \end{bmatrix} \quad (8)$$

where $[D]$ is a cyclosymmetric matrix:

$$A = \begin{bmatrix} 0 & 1 \\ \frac{k_t + 2k_c}{m} & 0 \end{bmatrix}, \qquad B = \begin{bmatrix} 0 & 0 \\ -\frac{k_c}{m} & 0 \end{bmatrix} \quad (9)$$

and k_t is the tuned or mean structural stiffness of the individual airfoils.

The eigenvalues of this block circular matrix $[D]$ can be expressed as eigenvalues of a 2×2 matrix Q_p:

$$\begin{aligned} Q_p &= D_1 + d_p D_2 + d_p^2 D_3 + \cdots + d_p^{N-1} D_N \\ &= \begin{bmatrix} 0 & 1 \\ \frac{k_t + 2k_c - k_c e^{i\frac{2\pi p}{N}} - k_c e^{i\frac{2\pi p(N-1)}{N}}}{m} & 0 \end{bmatrix} = \begin{bmatrix} 0 & 1 \\ \frac{k_t + 4k_c \sin^2(\pi p/N)}{m} & 0 \end{bmatrix} \end{aligned} \quad (10)$$

where $d_p = \exp(i2\pi p/N)$.

The eigenvalues of the Q_p matrices are

$$\omega_p = \sqrt{\frac{k_t + 4k_c \sin^2(\pi p/N)}{m}}, \qquad p = 0, 1, \ldots, N-1 \quad (11)$$

which represent the eigenvalues of the system matrix $[D]$ and, thus, the natural frequencies of the system with damping and aerodynamic effects neglected. Physically, the integer p is the nodal diameter of the mode shape.

For real rotors, Eq. (11) is a good approximation to the true resonant frequency because damping from both mechanical and aerodynamic sources is much less than the critical damping value.

The forced response of each airfoil is assumed to be harmonic at the forcing function frequency ω_r:

$$X_j(t) = x_j e^{i\omega_r t} \qquad j = 1, 2, \ldots, N \quad (12)$$

Equation (4) being forced at frequency ω_r thus becomes

$$\begin{aligned} &\cdots - \Gamma_j^{j-2} x_{j-2} - (k_c + \Gamma_j^{j-1}) x_{j-1} + (\delta k_j + 2k_c \cos\beta_r \\ &\quad + i\omega_r \bar{c} - \Gamma_j^j) x_j - (k_c + \Gamma_j^{j+1}) x_{j+1} \\ &\quad - \Gamma_j^{j+2} x_{j+2} - \cdots = F_o e^{i(j-1)\beta_r} \end{aligned} \quad (13)$$

where $\delta k_j = k_j - k_t$ is the mistuned stiffness of airfoil j, and Γ represents the following aerodynamic terms: $\Gamma_j^k = i\omega\rho u c[\widehat{C}_j^k]^L$ for bending, $\Gamma_j^k = \rho u^2 c^2 [\widehat{C}_j^k]^M$ for torsion, and $\Gamma_j^k = \rho u^2 c^2 [\widehat{C}_j^k]^{CW}$ for chordwise bending.

Equation (13) can be rewritten in matrix form as

$$\begin{bmatrix} \widehat{D}_1^1 & -(k_c+\Gamma_1^2) & -\Gamma_1^3 & \cdots & -(k_c+\Gamma_1^N) \\ -(k_c+\Gamma_2^1) & \widehat{D}_2^2 & -(k_c+\Gamma_2^3) & \cdots & -\Gamma_2^N \\ -\Gamma_3^1 & -(k_c+\Gamma_3^2) & \widehat{D}_3^3 & \cdots & -\Gamma_3^N \\ \vdots & \vdots & \vdots & \ddots & \vdots \\ -(k_c+\Gamma_N^1) & -\Gamma_N^2 & -\Gamma_N^3 & \cdots & \widehat{D}_N^N \end{bmatrix} \times \begin{Bmatrix} x_1 \\ x_2 \\ x_3 \\ \vdots \\ x_N \end{Bmatrix} = \begin{Bmatrix} F_0 \\ F_0 e^{i\beta_r} \\ F_0 e^{i2\beta_r} \\ \vdots \\ F_0 e^{i(N-1)\beta_r} \end{Bmatrix} \tag{14}$$

where $\widehat{D}_j^j = \delta k_j + 2k_c \cos\beta_r + i\omega_r \bar{c} - \Gamma_j^j$.

Solving the linear system of Eq. (14) for a given set of mistuned stiffnesses δk_j and aerodynamic and structural conditions yields the mistuned response of the system including unsteady aerodynamic effects.

IV. Unsteady Aerodynamic and Structural Effects

The importance of aerodynamic effects relative to the structural effects is ascertained by examination of Eq. (14). The structural or mechanical damping effect is the imaginary part of the diagonal term, that is, $\omega_r \bar{c}$. Aerodynamic damping results from the imaginary part of Γ_j^k and is present in every term in the coefficient matrix of Eq. (14). However, the diagonal Γ, that is, Γ_j^j is typically much larger than the off-diagonal Γ. Thus, a comparison of $\omega_r \bar{c}$ and $\mathrm{Im}(\Gamma_j^j)$ is a comparison of the relative importance of structural damping and aerodynamic damping. In terms of the nondimensional damping parameter, these two quantities are

$$\zeta^{\mathrm{mech}} = \frac{\bar{c}}{2m\omega_r} \qquad \zeta^{\mathrm{aero}} = -\frac{\mathrm{Im}(\Gamma_j^j)}{2m\omega_r^2} \tag{15}$$

If $\zeta^{\mathrm{mech}} \gg \zeta^{\mathrm{aero}}$, aerodynamic damping has little effect, whereas if $\zeta^{\mathrm{mech}} \ll \zeta^{\mathrm{aero}}$, aerodynamic damping has a large effect.

Structural coupling from airfoil to airfoil appears as k_c in Eq. (4), with these terms directly affecting the $j-1$ and $j+1$ airfoils. Thus, the extent to which the unsteady aerodynamics affects this airfoil-to-airfoil coupling is determined qualitatively by a comparison of k_c with the real parts of Γ_j^{j-1} and Γ_j^{j+1}, that is, the aerodynamic coupling stiffness of airfoil $j-1$ and $j+1$. Typically, unsteady aerodynamic coupling stiffnesses are much less than structural coupling stiffnesses, and so it is expected that only for extremely small structural airfoil-to-airfoil coupling will the unsteady aerodynamic coupling be important.

V. Partial Mistuning

As mistuning stiffnesses are generally not known during design, mistuning models are directed at finding the largest possible response given $-a < \delta k_j < a$, $j = 0, 1, \ldots, N-1$, with a some real number. Because the number of airfoils on a row can be large, the number of required solutions to the $N \times N$ system of Eq. (14) can be prohibitively large. For example, if 100 values of δk_j yields adequate resolution between $-a$ and a, then for a 72-bladed rotor, the 72×72 system of Eq. (13) must be solved 10^{144} times.

The partial-mistuning model mitigates this difficulty by reducing the number of airfoils on the row that needs be included, an approach that takes advantage of the mode localization phenomenon. Thus, for the present model it is necessary to consider only a sector of the annulus containing s airfoils such that $j \in [0, p] \cup [N-p, N-1]$ with $s = 2p+1$ typically much less than N, and p is any integer in $0 < p < N/2$.

The dynamic behavior of the tuned system, that is, $\delta k_j = 0$ for all j, plays a key role in the partial-mistuning solution. The tuned system response to unit forcing acting only on airfoil k is expressed as a vector of length N defined as $\underline{h}^k$. That is, $\underline{h}^k$ is the solution to

$$\cdots - \Gamma_j^{j-2} h_{j-2}^k - (k_c + \Gamma_j^{j-1}) h_{j-1}^k + (2k_c \cos\beta_r + i\omega_r \bar{c} - \Gamma_j^j) h_j^k - (k_c + \Gamma_j^{j+1}) h_{j+1}^k - \Gamma_j^{j+2} h_{j+2}^k - \cdots = \delta_{jk} \tag{16}$$

The matrix $\tilde{\boldsymbol{h}}$ is defined as the matrix for which the kth column is $\underline{h}^k$, that is, $\tilde{\boldsymbol{h}} = [\,\underline{h}^0 \quad \underline{h}^1 \quad \cdots \quad \underline{h}^{N-1}\,]$. Because the system is tuned and cyclosymmetric, $\underline{h}^{k+1}$ is equivalent to $\underline{h}^k$ with each element shifted down one and element N moved to element 1. Thus, $\tilde{\boldsymbol{h}}$ is determined by a single solution to the $N \times N$ linear system of Eq. (16) with $k = j$.

The mistuned system of equation, Eq. (13), is expressed in matrix form as

$$\tilde{\boldsymbol{H}}\,\underline{x} = \underline{F} \tag{17}$$

With partial mistuning, only a segment of the airfoils are directly affected by the mistuning, that is, their mistuning stiffnesses are not zero, whereas the rest of the airfoils have zero mistuning stiffness but are indirectly affected by mistuning. Accordingly, the solution vector is divided into two parts:

$$\underline{x} = \begin{Bmatrix} \underline{x}_d \\ \underline{x}_i \end{Bmatrix} \tag{18}$$

where d denotes directly affected by mistuning, and i denotes indirectly affected by mistuning.

Applying this division to Eq. (17) yields

$$\begin{bmatrix} \tilde{\boldsymbol{H}}_{dd} & \tilde{\boldsymbol{H}}_{di} \\ \tilde{\boldsymbol{H}}_{id} & \tilde{\boldsymbol{H}}_{ii} \end{bmatrix} \begin{bmatrix} \underline{x}_d \\ \underline{x}_i \end{bmatrix} = \begin{bmatrix} \underline{F}_d \\ \underline{F}_i \end{bmatrix} \tag{19}$$

The matrix $\tilde{\boldsymbol{H}}_{dd}$ is expressed as the sum of a tuned matrix and a mistuned counterpart, that is, $\tilde{\boldsymbol{H}}_{dd} = \tilde{\boldsymbol{H}}_{dd}^t + \boldsymbol{\Delta}\tilde{\boldsymbol{H}}_{dd}$. δk_j is zero in the other three submatrices, and so these are equivalent to their tuned system counterparts. Thus, Eq. (19) is rewritten as

$$\begin{bmatrix} \tilde{\boldsymbol{H}}_{dd}^t & \tilde{\boldsymbol{H}}_{di} \\ \tilde{\boldsymbol{H}}_{id} & \tilde{\boldsymbol{H}}_{ii} \end{bmatrix} \begin{bmatrix} \underline{x}_d \\ \underline{x}_i \end{bmatrix} = \begin{bmatrix} \underline{F}_d \\ \underline{F}_i \end{bmatrix} + \begin{bmatrix} -\boldsymbol{\Delta}\tilde{\boldsymbol{H}}_{dd}\,\underline{x}_d \\ 0 \end{bmatrix} \tag{20}$$

The coefficient matrix of the left-hand side is now equivalent to the tuned system coefficient matrix. The mistuned problem can thus be viewed as a tuned system responding to the two right-hand-side forcing functions. Based on this observation, the tuned system response to unit forcing on airfoil k, that is, $\underline{h}^k$, can be used as a basis for the solution to the mistuned system.

To illustrate, consider a right-hand-side forcing vector with elements f_j, $j = 0, 1, \ldots, N-1$. The linearity of the system then allows the solution to be written as $\sum_j f_j \underline{h}^j$.

By analogy, the solution to Eq. (20) is

$$\begin{bmatrix} \underline{x}_d \\ \underline{x}_i \end{bmatrix} = \tilde{\boldsymbol{h}} \left\{ \begin{bmatrix} \underline{F}_d \\ \underline{F}_i \end{bmatrix} + \begin{bmatrix} -\boldsymbol{\Delta}\tilde{\boldsymbol{H}}_{dd}\underline{x}_d \\ 0 \end{bmatrix} \right\} \tag{21}$$

The first term on the right-hand side is just the response of the tuned system to the external forcing. Taking the other term to the left-hand side yields

$$\begin{bmatrix} \underline{x}_d \\ \underline{x}_i \end{bmatrix} = \tilde{\boldsymbol{h}} \begin{bmatrix} \boldsymbol{\Delta}\tilde{\boldsymbol{H}}_{dd}\underline{x}_d \\ 0 \end{bmatrix} = \begin{bmatrix} \underline{x}_d^t \\ \underline{x}_i^t \end{bmatrix} \tag{22}$$

where the superscript on $\underline{x}$ denotes the tuned solution to external forcing.

An entirely equivalent representation is

$$\left[\boldsymbol{I}+\begin{bmatrix}\tilde{\boldsymbol{h}}_{dd} & \tilde{\boldsymbol{h}}_{di}\\ \tilde{\boldsymbol{h}}_{id} & \tilde{\boldsymbol{h}}_{ii}\end{bmatrix}\begin{bmatrix}\Delta\tilde{\boldsymbol{H}}_{dd} & \boldsymbol{0}\\ \boldsymbol{0} & \boldsymbol{0}\end{bmatrix}\right]\begin{bmatrix}\underline{x}_d\\ \underline{x}_i\end{bmatrix}=\begin{bmatrix}\underline{x}_d^t\\ \underline{x}_i^t\end{bmatrix} \tag{23}$$

where the $\tilde{\boldsymbol{h}}$ matrix has been segmented into four parts, entirely analogous to the $\tilde{\boldsymbol{H}}$ matrix segmentation.

The $\underline{x}_d$ vector is solved with

$$(\boldsymbol{I}+\tilde{\boldsymbol{h}}_{dd}\Delta\tilde{\boldsymbol{H}}_{dd})\underline{x}_d=\underline{x}_d^t \tag{24}$$

The vector $\underline{y}$ is introduced whose elements are $y_j=(x)_j/(x^t)_j$. This is the amplification factor vector because $|y_j|$ is the amplification of the mistuned system response divided by the tuned system response. In terms of the amplification factor, Eq. (24) is written as

$$(\boldsymbol{I}+\tilde{\boldsymbol{h}}_{dd}\Delta\tilde{\boldsymbol{H}}_{dd})\underline{y}_d=\underline{1} \tag{25}$$

where $\underline{1}$ is a vector of ones of length s.

Once $\underline{x}_d$ is known from Eq. (25), $\underline{x}_i$ is found from Eq. (22):

$$\underline{x}_i=\underline{x}_d^t-\tilde{\boldsymbol{h}}_{id}\Delta\tilde{\boldsymbol{H}}_{dd}\underline{x}_d \tag{26}$$

The mistuned matrix $\Delta\tilde{\boldsymbol{H}}_{dd}$ is the difference of the mistuned system matrix and the tuned system matrix, that is, the difference of the left-hand sides of Eqs. (12) and (15). Thus $\Delta\tilde{\boldsymbol{H}}_{dd}$ is a diagonal matrix for which the diagonal terms are δk_j.

As an example, consider the case in which only three airfoils are directly affected by mistuning, that is, $s=3$. Label the middle airfoil 0 and arrange the $\underline{x}_d$ vector as $\{x_{N-1}\quad x_0\quad x_1\}^T$. Then Eq. (25) is

$$\begin{bmatrix}1+h_0\delta k_{N-1} & h_{N-1}\delta k_0 & h_{N-2}\delta k_1\\ h_1\delta k_{N-1} & 1+h_0\delta k_0 & h_{N-1}\delta k_1\\ h_2\delta k_{N-1} & h_1\delta k_0 & 1+h_0\delta k_1\end{bmatrix}\begin{bmatrix}y_{N-1}\\ y_0\\ y_1\end{bmatrix}=\begin{bmatrix}1\\ 1\\ 1\end{bmatrix} \tag{27}$$

VI. Optimization

Designers want to know the worst-case mistuning, obtained by numerical optimization, that is, the set of δk values that maximize $|y_0|$. Optimization is performed with a FORTRAN-based direct search complex algorithm with limitation of upper and lower bounds. This optimizer uses the unconstrained nonlinear optimization scheme with the simplex search method, a direct search algorithm, to find a minimum point of a function of several variables [21]. Therefore, the maximum amplification factor and the airfoil mistuned stiffness distributions are obtained at the given structural and aerodynamic conditions.

VII. Results

A. Unsteady Aerodynamic Effects: Baseline

To demonstrate the effects of aerodynamic damping on mistuned rotor amplification factor, simulations are performed for the baseline rotor summarized in Table 1. The mistuned stiffness has $+0.1k_t$ upper and $-0.1k_t$ lower bounds resulting in a maximum $\pm 4.9\%$ change in natural frequency as compared to the tuned frequency.

B. Mistuning Sector Size, s

The validation of the partial-mistuning approximation is addressed for the baseline rotor by predicting the variation of the amplification factor with sector size s. The baseline case has 24 airfoils, with the mistuning sector size s specifying the number of airfoils directly affected by the mistuning.

Figure 4 shows the maximum amplification factor versus s for the baseline geometry and two mechanical damping ratios. Note that the mistuning stiffness δk_j is chosen randomly within the range between $-0.1k_t$ and $+0.1k_t$. Note that the aerodynamic damping factor for the baseline is $\zeta^{\text{aero}}=0.010$. For the mechanical damping ratio $\zeta^{\text{mech}}=0.01$, the results with and without unsteady aerodynamics, that is, with and without aerodynamic damping, have a similar dependence on s, with a 30% difference between the amplification factor for $s=3$ and 23. At a smaller damping ratio of $\zeta^{\text{mech}}=0.001$, the structure-only results converge rapidly, with only a 4% difference in results from $s=7$ to 23.

Including unsteady aerodynamics results in a much slower convergence, with a 15% difference in the amplification factor from $s=7$ to 23. At the smallest damping ratio, $\zeta^{\text{mech}}=0.001$, the amplification factors without unsteady aerodynamics also converge faster than those including the unsteady aerodynamics.

In a comparison of $s=3$ to 23 for the two damping ratios with unsteady aerodynamics, the differences in the amplification factor are 32 and 42%, respectively, as the damping ratio decreases.

In conclusion, the sector size s is an important parameter. Small sector sizes minimize the computational time requirements while providing qualitatively correct results. For high accuracy, on the order of one-half the number of blades in the rotor is required.

Table 1 Baseline rotor properties

Structural stiffness, k_t	3.708×10^3 N
Structural coupling, k_c	$0.1k_t$
Number of airfoils, N	24
Natural frequency, ω_r	600 Hz
SDOF mode	Torsion
Spacing-to-chord ratio	1.5
Stagger from axial	61.8 deg
Mach number	0.5
Reduced frequency	1.5633
Nodal diameter, ND	$N/4$
Elastic axis location	44.3% chord

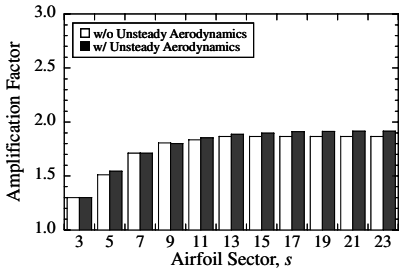

a) ζ^{mech} **= 0.01**

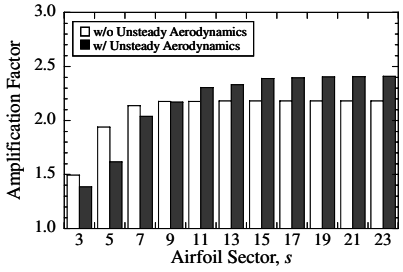

b) ζ^{mech} **= 0.001**

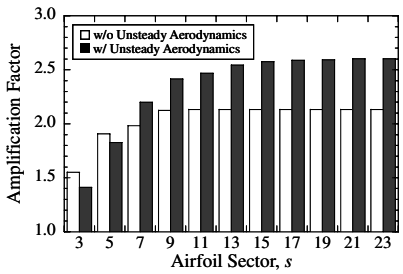

c) ζ^{mech} **= 0.0001**

Fig. 4 Maximum amplification factor dependence on s for three mechanical damping values.

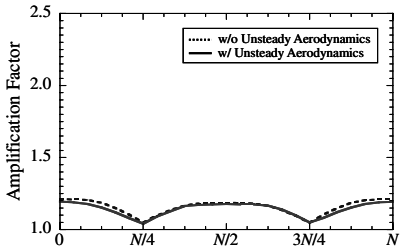

a) $\zeta^{mech} = 0.1$

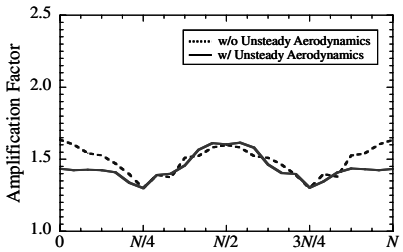

b) $\zeta^{mech} = 0.01$

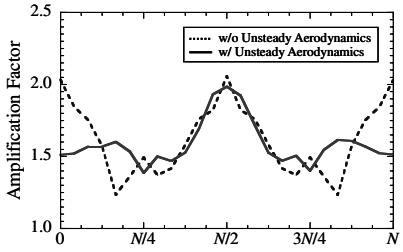

c) $\zeta^{mech} = 0.001$

Fig. 5 Varying structural damping with aerodynamic damping fixed.

C. Aerodynamic Damping Effects, $s = 3$

The aerodynamic damping factor for the baseline is $\zeta^{\text{aero}} = 0.0102$, nearly equal to the structural damping of 0.0100. Because $\zeta^{\text{aero}} \approx \zeta^{\text{mech}}$, it is expected that the aerodynamic damping has a noticeable effect. Note that, for this brief study, a sector size of $s = 3$ is used, selected to minimize the computational and time requirements. Although not ideal, this sector size does provide qualitatively correct results, as noted in the previous section. In Fig. 5, the aerodynamic conditions are held fixed while the structural damping is varied from 0.1 to 0.0001. Very large structural damping, $\zeta^{\text{mech}} = 0.1$, results in the lowest amplification factors. When $\zeta^{\text{mech}} = 0.1$, $\zeta^{\text{aero}} \ll \zeta^{\text{mech}}$ and the unsteady aerodynamics has relatively little effect on the amplification factor. The upper-right-hand plot is the baseline case, and the lower-left-hand plot has $\zeta^{\text{mech}} = 0.001$, so that $\zeta^{\text{aero}} \gg \zeta^{\text{mech}}$. In this case, the unsteady aerodynamics has a very large effect on the amplification factor, yielding as much as a 50% decrease in amplification factor at a zero nodal diameter of excitation and a 30% increase at a nodal diameter of $N/6$. Lowering the structural damping by another order of magnitude results in even larger differences between the with- and without-unsteady-aerodynamics results.

The effect of changing the aerodynamic damping while holding the structural damping fixed is shown in Fig. 6. Because ζ^{aero} is inversely proportional to ω_r^2, the aerodynamic damping ζ^{aero} is decreased by increasing ω_r, practically accomplished by increasing k_t. Increasing ω_r from the baseline of 600–4300 Hz results in $\zeta^{\text{aero}} \approx 0.001$. Because the structural damping is 0.01, the aerodynamic damping is almost negligible, so that including aerodynamics has little effect. Next, the aerodynamic damping is increased while again keeping the structural damping fixed at 0.01. The aerodynamic damping is increased to approximately 0.03 by decreasing ω_r to 250 Hz. The unsteady aerodynamics has a large effect on the amplification factor, increasing it by as much as 25% at a nodal diameter of $11N/16$.

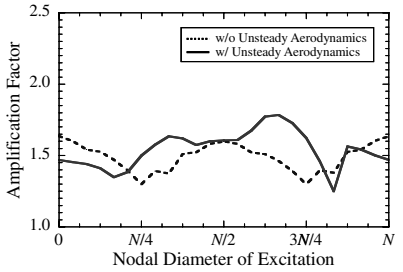

a) ω_r**= 250 Hz (k$_c$ = 0.6)**

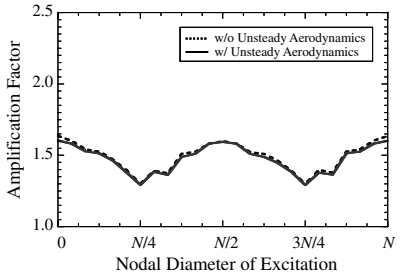

b) ω_r**= 4300 Hz (k$_c$ = 11.2)**

Fig. 6 Amplification factor at 250 and 4300 Hz ($k_c = 0.6$ and 11.2).

D. Purdue Transonic Axial Compressor

The mistuning analysis including unsteady aerodynamic effects developed herein is now applied to the geometry of an actual rotor, the IBR of the Purdue transonic axial compressor for the numerical simulation. This compressor has an 8.0 in. i.d. and a 12.0 in. o.d., with 20 inlet guide vanes, 18 rotor blades, and 20 stators. With 18 rotor blades and 20 vanes, the two nodal diameter excitation ($ND = 2$) is of interest. The bending mode resonant response with the 20E line occurs at 17,000 rpm. Assuming upstream stagnation properties at standard temperature and pressure, the rotor inlet relative Mach number is 0.84 at 90% span. A summary of the structural and aerodynamic properties of this IBR model is given in Table 2.

1. IBR Baseline Response

To show the importance of including unsteady aerodynamics in mistuning models and, hence, the need for the mistuning model developed herein, the baseline response of the IBR is analyzed. The airfoil second bending mistuning stiffness distribution determined from experimental bench testing is shown in Fig. 7. The IBR model can now be solved as an 18×18 system. Optimization is not performed because the mistuned stiffnesses are known.

Airfoil response amplitude versus the frequency for the 20E excitation with and without unsteady aerodynamics is shown in Fig. 8. The frequency is normalized by ω_2, the natural frequency of the second bend mode at $ND = 2$, with the amplitudes normalized by the maximum tuned amplitude without unsteady aerodynamics. A solid black line represents the tuned normalized amplitude. Note that,

Table 2 IBR structural and aerodynamic properties

Structural stiffness, k_t	6.48×10^8 N/m^2
Structural damping, ζ^{mech}	0.001
Structural coupling, k_c	$0.377k_t$
Coupling stiffness	$0.377k_t$
SDOF mode (for aero only)	Second bending
Spacing-to-chord ratio	1.018
Stagger from axial	64.72 deg
Mach number	0.84
Reduced frequency	6.36
Chord, c	0.05 m

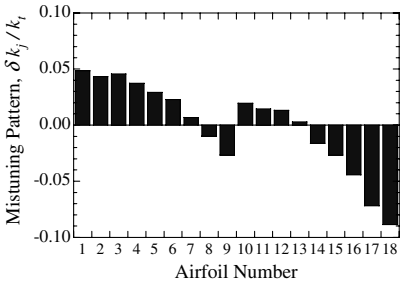

Fig. 7 Airfoil mistuning stiffness pattern.

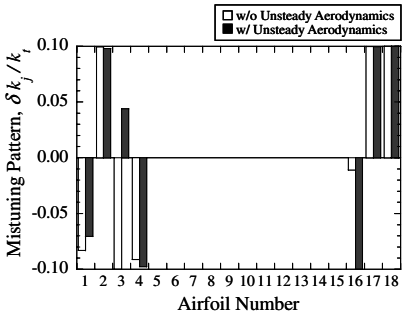

Fig. 9 Optimum mistuning stiffness pattern, $s = 7$.

for a tuned airfoil row, the 20E excitation is orthogonal to all mode shapes except the $2ND$ mode shape. Thus, only one peak appears. In contrast, the mistuned results have several peaks in the frequency range of 0.96–1.04, a consequence of the distortion of mode shapes caused by mistuning. The natural mode shapes are distorted and the 20E excitation has nonzero projections onto these mode shapes with mistuning. As a result, all modes contribute to the response at their respective natural frequencies. The double peak near $\omega/\omega_2 = 1.0$ is the perturbed $2ND$ mode shape and the perturbed $16ND$ mode shape, both of which have natural frequencies close to 1.0.

For the tuned rotor, the ratio of the maximum tuned amplitude with unsteady aerodynamics to that without is 0.5580. This is a result of the additional damping originating from the unsteady aerodynamic effects. For this case, the mechanical and aerodynamic damping are equal, that is, $\zeta^{\text{mech}} = 0.001 = \zeta^{\text{aero}}$.

For the tuned IBR, the ratio of the maximum amplitude with unsteady aerodynamics to that without is 0.5580. For the mistuned rotor, airfoil 4 has the peak response amplitude both with and without unsteady aerodynamics at $\omega/\omega_2 = 0.997$. The ratio of the maximum amplitude with unsteady aerodynamics to that without for airfoil 4 is 0.488. Also, including aerodynamic damping is of primary importance whereas the mistuning is only of secondary importance, with the ratio of the maximum amplitude with unsteady aerodynamics of the tuned to mistuned IBRs approximately 0.93.

2. *IBR Optimal Response*

The partial-mistuning optimization model is now applied to the IBR to determine the optimum mistuning stiffness pattern. First, the partial-mistuning analysis with $s = 7$ is used and the effects of unsteady aerodynamics on the maximum response and optimized mistuning stiffness pattern analyzed. Second, to investigate the confidence of the partial-mistuning optimization model, the full-mistuning optimization model is also applied.

Figure 9 shows the optimum mistuning stiffness pattern with $s = 7$. Zero mistuning for airfoils 5–15 is a consequence of the partial-mistuning model, wherein airfoils far from airfoil 1 are assumed to be tuned.

The tuned and mistuned resonant response amplitudes and the corresponding normalized response on each blade at $\omega/\omega_2 = 1.0$ for these optimal mistuning stiffness patterns are investigated. First, the importance of including or not including unsteady damping on the IBR blade-to-blade amplitude distributions and maximum response is considered. The response of each blade determined with aerodynamic damping included for an IBR with an optimal mistuning stiffness pattern determined with unsteady aerodynamics, that is, the optimally designed IBR, is then presented.

Figure 10 presents the normalized response of each blade with and without unsteady aerodynamics, that is, aerodynamic damping, for the IBR optimal mistuning stiffness pattern determined without unsteady aerodynamics. Clearly seen is that including aerodynamic damping significantly alters the response blade-to-blade distribution and amplitudes. Whereas a number of individual blades have relatively high amplitudes and a number have relatively low amplitudes, that is, an irregular spiked response distribution without aerodynamic damping, this is not the case when aerodynamic damping is included. With aerodynamic damping, the distribution is relatively smooth, with only blades 1 and 18 having somewhat high relative amplitudes. Also, blade 1 exhibits the maximum mistuned normalized amplitude both with and without aerodynamic damping, with this maximum of 1.54 without unsteady aerodynamics decreasing to 0.79 with unsteady aerodynamics.

Figure 11 shows the response of the optimally designed IBR. Presented is the normalized response of each blade predicted, including aerodynamic damping for an IBR with an optimal mistuning stiffness pattern determined with unsteady aerodynamics. Also shown for ease of comparison are the previously presented corresponding results predicted with aerodynamic damping for the IBR optimized without aerodynamic damping. The predicted blade-to-blade response results for the two cases are similar, with relatively smooth blade-to-blade mistuning patterns and only blades 1 and 18 having notably high responses. However, there are blade-to-blade differences in the individual blade amplitudes. Blade 18 has a higher

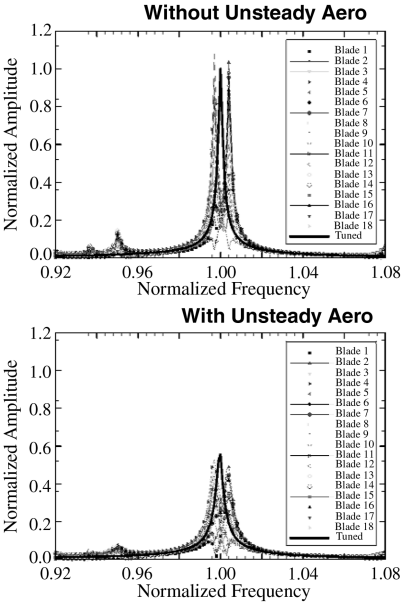

Fig. 8 Tuned and mistuned normalized amplitude with and without unsteady aerodynamics.

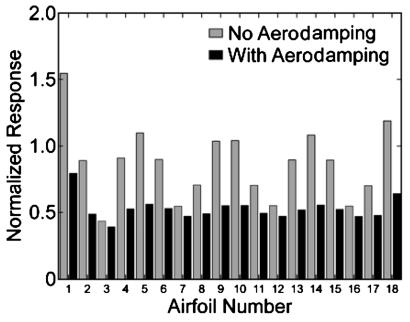

Fig. 10 Normalized response for optimal mistuning determined without unsteady aerodynamics, $s = 7$.

response for the IBR optimized without aerodynamic damping than that optimized with aerodynamic damping. Blade 1 exhibits the maximum mistuned normalized response, 0.8730 for the optimally designed IBR as compared to 0.79 for the IBR optimized without aerodynamic damping.

E. IBR Optimal Response Verification

The full-mistuning optimization model is applied to the IBR to demonstrate the validity of the partial-mistuning optimization model results. Figures 12 and 13 show the full-mistuning optimum mistuning stiffness pattern and the corresponding resonant response, analogous to the partial-mistuning optimizer $s = 7$ results.

The optimum mistuning stiffness from the full-mistuning optimizer has a pattern different from the partial-mistuning optimized pattern. After full-mistuning optimization, the maximum mistuned amplitude occurs at airfoil 1, with this maximum at 1.7307 without unsteady aerodynamics and at 0.9333 with unsteady aerodynamics. These maximum amplitudes are compared to the partial-mistuning maximum amplitudes in Table 3. For $s = 17$, the maximum amplitude without aerodynamics is 2% larger than that achieved with the full-mistuning model, with this maximum at 1.7682. With aerodynamics, the $s = 17$ and full-mistuning normalized amplitudes are identical to the second decimal place.

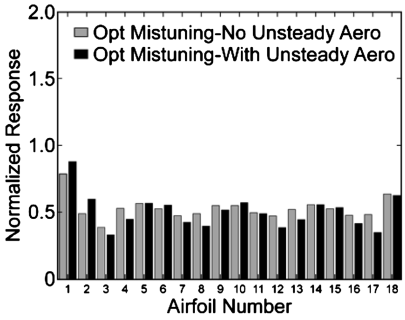

Fig. 11 Normalized response with unsteady aerodynamics for the optimal mistuning stiffness patterns.

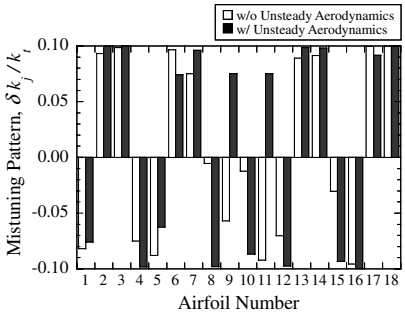

Fig. 12 Optimum mistuning stiffness pattern.

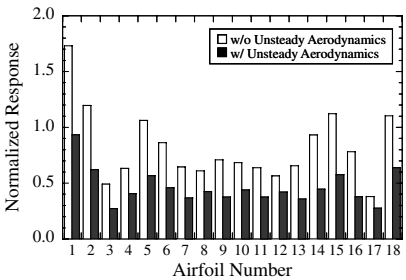

Fig. 13 Optimized mistuned normalized response after full-mistuning optimization.

Table 3 Optimized normalized amplitudes for IBR

	Max Normalized Amplitude	
	W/o unsteady aerodynamics	W/ unsteady aerodynamics
$s = 7$	1.54	0.87
$s = 17$	1.77	0.93
Full mistuning	1.73	0.93

VIII. Conclusions

A mistuning model has been developed that includes aerodynamic damping. LINSUB, an inviscid linearized unsteady aerodynamic damping code, provides the unsteady aerodynamic coefficients that are converted to influence coefficients suitable for incorporation into the mistuning model.

Aerodynamic damping has a large effect on the mistuned amplification factor when the aerodynamic damping is nonnegligible compared to the structural damping. The aerodynamic damping parameter ζ^{aero} provides qualitative knowledge of how much unsteady aerodynamics will influence the mistuned amplification factor. If ζ^{aero} is approximately equal to or larger than the mechanical damping ζ^{mech}, aerodynamics plays an important role in the result. If $\zeta^{\text{aero}} \ll \zeta^{\text{mech}}$, the inclusion of aerodynamics will have little effect. This is of particular importance for IBRs. Namely, the mechanical damping is considerably reduced in IBRs, with this analysis having demonstrated that aerodynamic damping is significant when the mechanical damping is small. Thus, it is necessary to consider aerodynamic damping in the vibratory stress analysis of mistuned IBRs.

A realistic IBR was analyzed that showed if unsteady aerodynamics are neglected, the computed optimal mistuning pattern is not optimum in the actual operating environment wherein unsteady aerodynamic effects are present. Whether or not unsteady aerodynamics should be included in the mistuning analysis again depends on the comparison of the aerodynamic damping and the mechanical damping.

Acknowledgment

This research was sponsored, in part, by the U.S. Air Force Office of Scientific Research. This support is most gratefully acknowledged.

References

[1] Whitehead, D. S., "Effect of Mistuning on the Vibration of Turbomachine Blades Induced by Wakes," *Journal of Mechanical Engineering Science*, Vol. 8, No. 1, 1966, pp. 15–21. doi:10.1243/JMES_JOUR_1966_008_004_02

[2] Whitehead, D. S., "The Maximum Factor by Which Forced Vibration of Blades Can Increase Due to Mistuning," *Journal of Engineering for Gas Turbines and Power*, Vol. 120, No. 1, 1998, pp. 115–119. doi:10.1115/1.2818061

[3] Kenyon, J., and Griffin, J., "Harmonic Mistuning of Turbine Engine Bladed Disks and Implications on Sensitivity to Forced Response," American Society Of Mechanical Engineers Paper 2001-GT-0274, June 2001.

[4] Sinha, A., "Computation of Maximum Amplitude of a Mistuned Bladed Disk Assembly via Infinity Norm," *Proceedings of the ASME Aerospace Division*, Vol. AD-55, 1997, pp. 427–432.

[5] Petrov, E., and Ewins, D., "Analysis of the Worst Mistuning Patterns in Bladed Disc Assemblies," American Society Of Mechanical Engineers Paper 2001-GT-0293, June 2001.

[6] Rivas-Guerra, A. J., and Mignolet, M. P., "Maximum Amplification of Blade Response Due to Mistuning: A Localization-Based Optimization," *Journal of Turbomachinery*, Vol. 125, No. 3, 2003, pp. 442–454. doi:10.1115/1.1506958

[7] Choi, Y., Gottfried, D. A., and Fleeter, S., "Aerodynamic Effects on Mistuned Bladed Disks," AIAA Paper 3639, July 2002.

[8] Kaza, K. R. V., and Kielb, R. E., "Flutter and Response of a Mistuned Cascade in Incompressible Flow," *AIAA Journal*, Vol. 20, No. 8, 1982, pp. 1120–1127. doi:10.2514/3.51172

[9] Kielb, R. E., and Kaza, K. R. V., "Effects of Structural Coupling on Mistuned Cascade Flutter and Response," *Journal of Engineering for Gas Turbines and Power*, Vol. 106, No. 1, 1984, pp. 17–24. doi:10.1115/1.3239532

[10] Basu, P., and Griffin, J. H., "The Effect of Limiting Aerodynamic and Structural Coupling in Models of Mistuned Bladed Disk Vibration," *Journal of Vibration, Acoustics, Stress, and Reliability in Design*, Vol. 108, No. 2, 1986, pp. 132–139.

[11] Pierre, C., and Murthy, D. V., "Aeroelastic Modal Characteristics of Mistuned Blade Assemblies: Mode Localization and Loss of Eigenstructure," *AIAA Journal*, Vol. 30, No. 10, 1992, pp. 2483–2496. doi:10.2514/3.11251

[12] Pierre, C., Smith, T. E., and Murthy, D. V., "Localization of Aeroelastic Modes in Mistuned High-Energy Turbines," *Journal of Propulsion and Power*, Vol. 10, No. 3, 1994, pp. 318–328. doi:10.2514/3.23759

[13] Kenyon, J. A., Rabe, D. C., and Fleeter, S., "Aerodynamic Effects on Blade Vibratory Stress Variations," *Journal of Propulsion and Power*, Vol. 15, No. 5, 1999, pp. 675–680. doi:10.2514/2.5492

[14] Lim, S., Bladh, R., Castanier, M. P., and Pierre, C., "A Compact, Generalized Component Mode Mistuning Representation for Modeling Bladed Disk Vibration," *Proceedings of the AIAA/ASME/ASCE/AHS/ASC Structures, Structural Dynamics and Materials Conference*, Vol. 2, AIAA, Reston, VA, 2003, pp. 1359–1380.

[15] Yang, M. T., and Griffin, J. H., "A Reduced-Order Model of Mistuning Using a Subset of Nominal System Modes," *Journal of Engineering for Gas Turbines and Power*, Vol. 123, No. 4, 2001, pp. 893–900. doi:10.1115/1.1385197

[16] Kielb, R. E., Feiner, D. M., Griffin, J. H., and Miyakozawa, T., "Flutter of Mistuned Bladed Disks and Blisks with Aerodynamic and FMM Structural Coupling," *Proceedings of the 2004 ASME Turbo Expo*, Vol. 6, American Society of Mechanical Engineers, New York, 2004, pp. 573–579.

[17] He, Z., Epureanu, B. I., and Pierre, C., "Effects of Unsteady Aerodynamics on the Dynamic Response of Mistuned Bladed Disks," *Proceedings of the Third MIT Conference on Computational Fluid and Solid Mechanics, Computational Fluid and Solid Mechanics*, edited by K. J. Bathe, Vol. 1, Elsevier, New York, 2005. pp. 250–255.

[18] Whitehead, D. S., "Classical Two-Dimensional Methods," *AGARD Manual on Aeroelasticity in Axial Flow Turbomachines (AG-298)*, AGARD, Vol. 1, Chap. 2, AG-298, 1987.

[19] Hoyniak, D., and Fleeter, S., "Aerodynamic and Structural Detuning of Turbomachine Supersonic Unstalled Torsion Flutter," *Journal of Propulsion and Power*, Vol. 2, No. 2, March–April 1986, pp. 161–167. doi:10.2514/3.51254

[20] Buffum, D., and Fleeter, S., "Investigation of Oscillating Cascade Unsteady Aerodynamics by an Experimental Influence Coefficient Technique," *Journal of Propulsion and Power*, Sept.–Oct. 1990, pp. 612–660. doi:10.2514/3.23262

[21] Belegunda, A. D., and Chandrupatla, T. R., *Optimization Concepts and Applications in Engineering*, Prentice–Hall, Upper Saddle River, NJ, 1999.

F. Liu
Associate Editor